FISEVIER

#### Contents lists available at ScienceDirect

# **Next Materials**

journal homepage: www.sciencedirect.com/journal/next-materials



#### Research article



# An acid-etched low-Pt high-entropy alloy with significantly boosted activity for alkaline hydrogen evolution

Bin Liu <sup>a,b,\*</sup>, Shiping Chen <sup>a</sup>, Weihao Tan <sup>a</sup>, Kezhen Zhang <sup>a</sup>, Xiao Xu <sup>a</sup>, Kun Dong <sup>a</sup>, Lan Yu <sup>a,\*\*</sup>, Kangcheung Chan <sup>b</sup>, Zhi Ren <sup>c,\*\*</sup>

- a Faculty of Materials Science and Engineering, Kunming University of Science and Technology, Kunming, Yunnan 650000, PR China
- b Advanced Manufacturing Technology Research Centre, Department of Industrial and Systems Engineering, The Hong Kong Polytechnic University, Hong Kong
- <sup>c</sup> School of Science, Westlake University, Hangzhou, Zhejiang 310024, PR China

#### ARTICLE INFO

# Keywords: Low-Pt high-entropy alloys Alkaline hydrogen evolution reaction Electrocatalyst Acid etching Catalytic activity

#### ABSTRACT

High-entropy alloys (HEAs) have attracted wide attention in the field of electrocatalysis owing to their tunable catalytic activity, multielement synergy and high stability. However, it remains challenging to develop efficient HEA catalysts for the alkaline hydrogen evolution reaction (HER) due to their vast multielement space and unidentified active sites. Herein, we report the synthesis and characterization of a low-Pt  $Nb_{35}V_{30}Mo_{10}Cu_{10}Pt_{15}$  HEA catalyst by combining arc-melting and acid etching. Remarkably, the acid-etched HEA exhibits an ultralow overpotential of 28 mV and a small Tafel slope of 40.9 mV dec<sup>-1</sup> at 10 mA cm<sup>-2</sup> in 1.0 M KOH solution, comparable with the commercial Pt/C catalyst. First principles calculations show that the enhanced catalytic performance is due to the significant reduction of the energy barrier for breaking the H-OH bond from the multiactive sites. Our work demonstrates that the combination of multisite synergy and acid-induced surface modification provides a novel strategy to develop efficient catalysts for alkaline HER.

#### 1. Introduction

Hydrogen energy has been widely accepted as one of the most prospective clean energy alternatives to the traditional fossil energy owing to its high energy density and zero-carbon emission, which is of great significance to relieve the global energy dilemma and environmental pollution [1-3]. In this context, electrocatalytic water splitting has drawn great attention as an economy and sustainable technology for efficient hydrogen production [4,5]. Nevertheless, the rection kinetics of electrocatalytic hydrogen evolution reaction (HER) highly affect the overall water splitting efficiency. In particular, the HER in alkaline medium suffers from a sluggish reaction kinetics and high energy barrier due to the additional water dissociation, which becomes a practical obstacle to the alkaline water electrolysis [6.7]. To overcome this problem, a larger number of electrocatalysts have been developed for the alkaline HER [8,9]. While Pt-based catalysts have been demonstrated to be the most effective catalysts for alkaline HER, their large-scale application is limited by the high-cost, scarcity, and poor durability in alkaline electrolyte [10]. It is thus highly desirable to

explore low-Pt or free-Pt catalysts to maximize the intrinsic activity and enhance the catalytic stability towards alkaline HER.

Alloying Pt with transition elements is known to be effective in boosting the intrinsic activity while simultaneously reducing the Pt usage [11,12]. For instance, in Pt-Ni alloyed bimetallic catalyst, the d-band center of the Pt active sites is shifted downward, which lowers the Gibbs free energy toward the hydrogen intermediates in alkaline HER [13]. However, traditional bimetallic or ternary Pt-based alloy catalysts tend to be phase-separated because of the large immiscible gaps of the constituted elements, making it difficult to realize the continuous regulation of the surface electronic structure [14,15]. In this regard, high-entropy alloys (HEAs), which incorporates four or more elements in a homogeneous solid solution structure, can effectively avoid this limitation under the high-entropy configuration [16–18]. Moreover, this multielement composition broadens the compositional space, and affords diverse adsorption sites to optimize the adsorption energy between intermediates and active sites, thus promoting the catalytic efficiency [19,20]. In addition, the entropy stabilization and sluggish diffusion of atoms hinder the degradation and corrosion of HEA

E-mail addresses: bliu0201@foxmail.com (Bin Liu), yulan000@hotmail.com (L. Yu), renzhimat@foxmail.com (Z. Ren).

<sup>\*</sup> Corresponding author at: Faculty of Materials Science and Engineering, Kunming University of Science and Technology, Kunming, Yunnan 650000, PR China. \*\* Corresponding authors.

catalysts [18,21].

Nonetheless, the complexity and random distribution of multiple elements also pose challenges in the exploration of efficient HEA catalysts. On one hand, it is hard to predict the HEA catalysts with desirable crystal structure via random combinations of various metal elements [22,23]. On the other hand, the compositional elements and surface structure of HEAs closely affect the catalytic activity. The homogeneous HEAs based on extremely non-equilibrium synthesis would restrict the structural flexibility and cause the loss of distinctive catalytic sites as well as the scarcity of surface sites [24,25]. Especially, the noble metal atoms as the potential active sites are often located inside HEA nanoparticles, which inevitably inhibits the catalytic activity [26]. As such, traditional homogeneous HEAs often require tailored surface structures or delicate morphological control to optimize their performance in specific reactions. As is well known, acid etching is a widely used technique to tailor the surface structures with exposed active sites,

thereby creating a hierarchical and functional surface to boost the catalytic capacities [27,28]. For example, Maulana et al. observed that acid-etched IrFeCoNiCu HEA undergoes surface reconstruction, leading to the formation of an Ir-enriched active shell with distinct nanodomain due to the preferential dissolution of 3d metals [29]. Meanwhile, the core retains a uniform single-phase HEA structure, which avoids the phase separation or elemental segregation that could affect the catalytic performance.

In this work, we elaborately design a low-Pt  $Nb_{35}V_{30}Mo_{10}Pt_{15}Cu_{10}$  HEA by alloying Pt with transition elements V, Nb, Mo and Cu, in which Pt is used as the H activation center, oxyphilic Mo as the OH interaction site to promote dissociation of water molecules [10], and Nb, V and Cu elements are adopted to balance the valence electron accounts for constructing an A15-type cubic phase HEA [30,31], as well as regulate the electronic state density by the electronegativity difference. In addition, to expose the internal Pt-based active sites and improve the

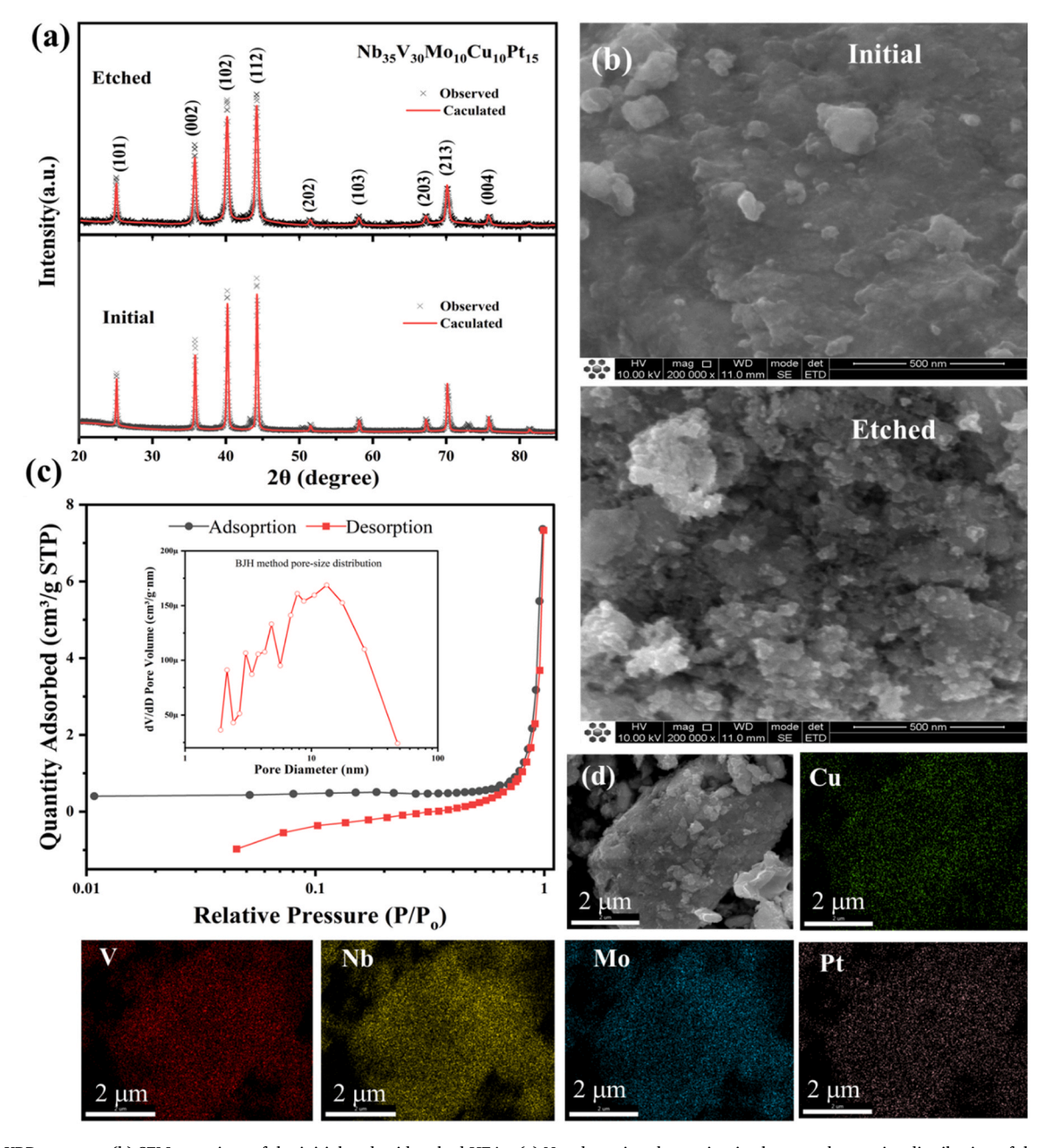


Fig. 1. (a) XRD patterns. (b) SEM mappings of the initial and acid-etched HEAs. (c) N<sub>2</sub> adsorption-desorption isotherm and pore-size distribution of the acid-etched Nb-V-Mo-Pt-Cu HEA. (d) Element distribution of the acid-etched Nb-V-Mo-Pt-Cu HEA.

atomic utilization efficiency, a simple acid etching process is adopted to modify the HEA surface by selectively removing a small quantity of V and Nb elements with relatively low reduction potential. Such a design highlights the importance of exposing Pt-based active sites on surface, while maintaining the strong synergistic catalytic effects to obtain efficient and durable catalysis. Indeed, the HEA after acid etching achieves a low overpotential of 28 mV@10 mA cm $^{-2}$  and a small Tafel slope of 40.9 mV dec $^{-1}$ , along with excellent durability in 1.0 M KOH solution. DFT investigations reveal that multielement synergy of HEA results in not only a higher density of electronic states distribute near the Fermi level ( $E_{\rm F}$ ) but also a lower energy barrier toward the water dissociation, which greatly accelerates the efficiency of water dissociation.

#### 2. Results and discussion

# 2.1. Preparation and structural characterizations

The Nb-V-Mo-Pt-Cu HEA catalyst was synthesized via the arcmelting method, followed by acid etching process. The synthesis details are summarized in the Experimental Section (Figure S1, Supplementary Materials). To confirm the optimal etching condition, we tested the polarization curves of this HEA catalyst with different etching times. As shown in Figure S2, the HEA after etching in HF for 10 min shows the lowest HER overpotential. As the etching time is increased to 20 min, the overpotential remains almost constant. However, further extending the etching time to 30 min leads to an increase in the HER overpotential, which is possibly because the elements loss or structural collapse originated from the excessive etching reduces the multicomponent synergetic effects and catalytic activity [32].

Fig. 1a shows the XRD patterns of the HEA before and after the acid etching. Very similar diffraction peaks are observed and can be well indexed on a cubic lattice with a *Pm-3n* space group (PDF#00–017–0711) [33]. The refined lattice constants are 5.015 Å and 5.018 Å, respectively, for the sample before and after acid etching. Moreover, the acid etching turns out to be effective in removing the impurity phases, which are marked by the asterisks. From the SEM image displayed in Fig. 1b, the initial HEA has a smooth surface, while the acid-etched HEA forms a loosened morphology covered with lots of ultrafine particles owning to the selective etching of V and Nb elements.

This is beneficial for exposing the internal active sites and increasing the specific surface area. The surface area and pore distribution of the etched HEA were investigated using Brunauer-Emmett-Teller (BET) analysis. As shown in Fig. 1c, the  $N_2$  adsorption-desorption test verified that it has a BET surface area of 1.91  $\mathrm{m}^2/\mathrm{g}$ , and shows a mesoporous structure with an average nanopore size of 21.7 nm. These abundant mesopores can facilitate mass transfer, such as the rapid release of  $H_2$  bubbles, and keep the catalyst exposed to the reactants, thus holding high catalytic activity [34].

Fig. 1d and Figure S3 show the elemental mappings obtained from the EDS measurement, and the corresponding atomic percentages are listed in Table S1. For both before and after acid etching, the constituent elements are distributed uniformly in the HEA without phase segregation and element aggregation. The measured composition of the initial HEA is consistent with the nominal one of  $Nb_{35}V_{30}Mo_{10}Cu_{10}Pt_{15}$ . After the acid etching, the atomic percentages of Nb and V elements decrease obviously (Nb:27.07 %, V:26.34 %), while Mo, Cu and Pt elements with low metal activity increase accordingly (Mo:10.13 %, Cu:14.45, Pt:22.01 %). These atomic percentages are also in consistent with the results of the ICP-OES test, and still meets the requirements of highentropy alloy composition (5 %-35 at%), maintaining a homogeneous high-entropy configuration ( $\Delta S:1.55$  R).

Fig. 2a shows the bright-field high-solution TEM image of the acidetched HEA, with regions A and B selected to analyze the microstructure. The selected area electron diffraction (SAED) patter of region A indicates a polycrystalline nature (Fig. 2b). Moreover, the diffraction rings match well with the XRD data, confirming its cubic structure. Fig. 2c presents the enlarged lattice fringe of region A, and gives an interplanar spacing of 0.213 nm. This spacing corresponds to the (112) crystal plane of the bcc structure, which is consistent with the fast Fourier transform (FFT) pattern (Fig. 2f). Notably, the crooked lattice fringes in Fig. 2e imply the sever lattice distortion from the large difference in the sizes of atoms existed in the acid-etched HEA. In the crystalline region B, multiple stacking faults and lattice distortion are also discernible (Fig. 2d). There structural defects induce surface strain effects, which contribute to optimizing the interaction between the actives sites and hence boosting the catalytic activity [35,36].

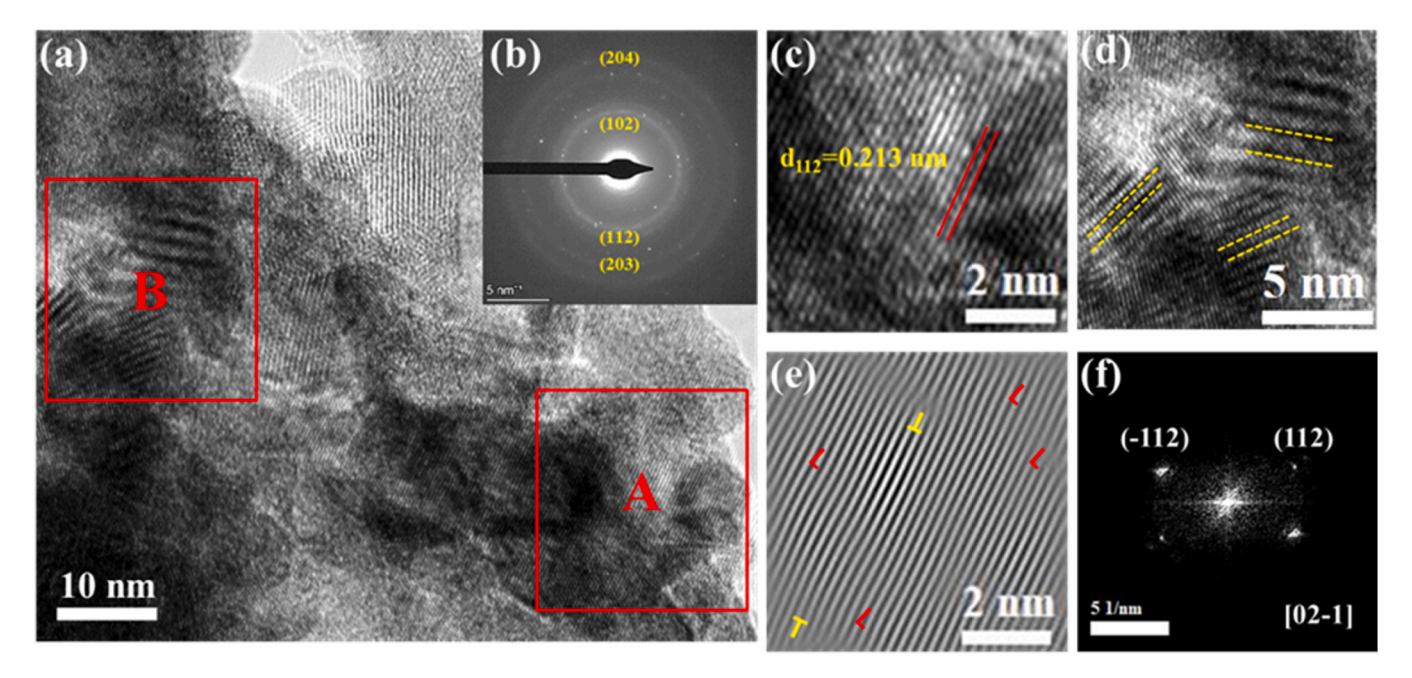


Fig. 2. (a) The bright-field TEM image. (b) The corresponding SAED pattern. (c) The enlarged image of region A. (d) The enlarged TEM image of region B. (e) Atomic lattice image of region A imaged along the (112) crystal plane. (f) FFT pattern of region A.

#### 2.2. Surface chemical valence states

The chemical valence states of the HEA before and after the acid etching are also studied by the XPS. The full XPS spectrum shown in Figure S4 confirms the coexistence of Nb, Mo, V, Pt, Cu and O elements on surface. Compared with the initial HEA, the peak intensities of V, Nb elements reduce after acid etching, while that of the Pt element increases significantly. These results are consistent with the EDS ones and imply that more Pt-based active sites are available on surface. Fig. 3 displays the XPS patterns of Pt 4 f, Mo 3d, Nb 3d, Cu 2p, V 2p, and O 1 s of the initial and etched HEAs. For the initial HEA, the Nb, V and Mo active metals with high oxygen affinity mainly form the highest oxidation states of Nb $^{5+}$ (207.2 eV), V $^{5+}$  (517.3 eV) and Mo $^{6+}$ (232.4 eV), respectively, due to surface oxidation. In comparison, Cu (935.1/933.1 eV) and Pt (73.8/71.5 eV) are found to be in the mixed valence states of 0 and 2<sup>+</sup>. After acid etching, the zero valence V<sup>0</sup> (520.4 eV) and Mo<sup>0</sup> (227.8 eV) are detected while the fractions of zero valence Cu<sup>0</sup> and Pt<sup>0</sup> increase, which is attributed to that the acid etching reveals the internal metallic states. On the other hand, the O1s spectrum suggests the binding energies at 530.5, 531.9 and 533.2 eV should correspond to the M-O, M-OH, and absorbed O species, respectively [37]. Note that the Mo, Nb and V elements after acid etching exhibit slightly negative shift at the binding energy, M-OH and M-O species show lightly positive shifts, signifying that the acid etching induces an enhanced electron hybridization in the Nb-V-Mo-Pt-Cu HEA [38,39].

#### 2.3. Alkaline HER performance

The alkaline HER performance of the initial and acid-etched HEAs is evaluated in 1.0 M KOH solution. As illustrated in Figs. 4a and 4b, the acid-etched HEA exhibits a high catalytic activity and rapid reaction kinetics for the alkaline HER. It only requires an overpotential of 28 mV to drive a current density of 10 mA cm $^{-2}$ , along with a low Tafel slope of 40.9 mV dec $^{-1}$ , which is much superior to the initial HEA (151 mV, 195.5 mV dec $^{-1}$ ) and comparable to the commercial Pt/C (32 mV, 47.1 mV dec $^{-1}$ ) catalyst under the same conditions. This is further corroborated by the comparison between the alkaline HER performance

of the representative noble-metal HEA catalysts and transition metalbased catalysts in Fig. 4c (corresponding overpotentials and Tafel slopes are summarized in Table S2). Indeed, such low overpotential and Tafel slope of the acid-etched Nb-V-Mo-Pt-Cu HEA can be comparable to or better than those state-of-the-art alkaline HER catalysts [40–46]. It is worth noting that the Pt content in this HEA catalyst is much lower than that of the noble metal-based HEA catalysts such as Pt<sub>4</sub>FeCoNiCu [41], PtMoPdRhNi [42] and CoNiMoPtRu [43]. Although these catalysts achieved excellent catalytic activity in the alkaline HER, the substantial use of precious metals and intricate nanostructures dramatically increased both the catalyst cost and preparation complexity. In contrast, the current HEA catalyst demonstrates a simplified composition design and synthesis process while maintaining high catalytic performance. Furthermore, this HEA catalyst obtains good stability with a small overpotential amplifications after working  $\sim$ 72 h in alkaline conditions at a static current density of 10 mA cm<sup>-2</sup>, even 20 mA cm<sup>-2</sup> (Fig. 4 f), outperforming most comparable catalysts and commercial Pt/C catalyst [44]. More importantly, the previously reported HEA nanocatalysts are generally prepared by solution-type or shock-type syntheses, which often suffered from the poor generality or harsh high temperature conditions [47,48]. All these issues can be avoided in this synthesis procedure employed in the present study, which may also benefit the large-scale production.

The HER performance of the initial and acid-etched HEAs is further characterized by the electrochemical impedance spectroscopy (EIS) and cyclic voltammetry (CV) method. As can be seen from the Nyquist plots shown in Fig. 4d, the Nb-V-Mo-Pt-Cu HEA after acid etching shows better interfacial charge-transfer kinetics in alkaline HER than both the initial HEA and Pt/C [49]. Meanwhile, the double-layer capacitance ( $C_{\rm dl}$ ) measured via the CV method in the non-faradaic region at different scan rate is 3.84 mF cm<sup>-2</sup> for the acid-etched HEA (Figure S5). This value is higher than those of the Pt/C (3.18 mF cm<sup>-2</sup>) and initial HEA (2.12 mF cm<sup>-2</sup>) (Fig. 4e), implying that the acid etching induces an increased electrochemical active surface area (ECSA) [50]. We further investigated the intrinsic HER activity by normalizing the LSV curves with respect to the calculated ECSA (Figure S6), the results revealed that the overpotential of the etched HEA is substantially lower than that of

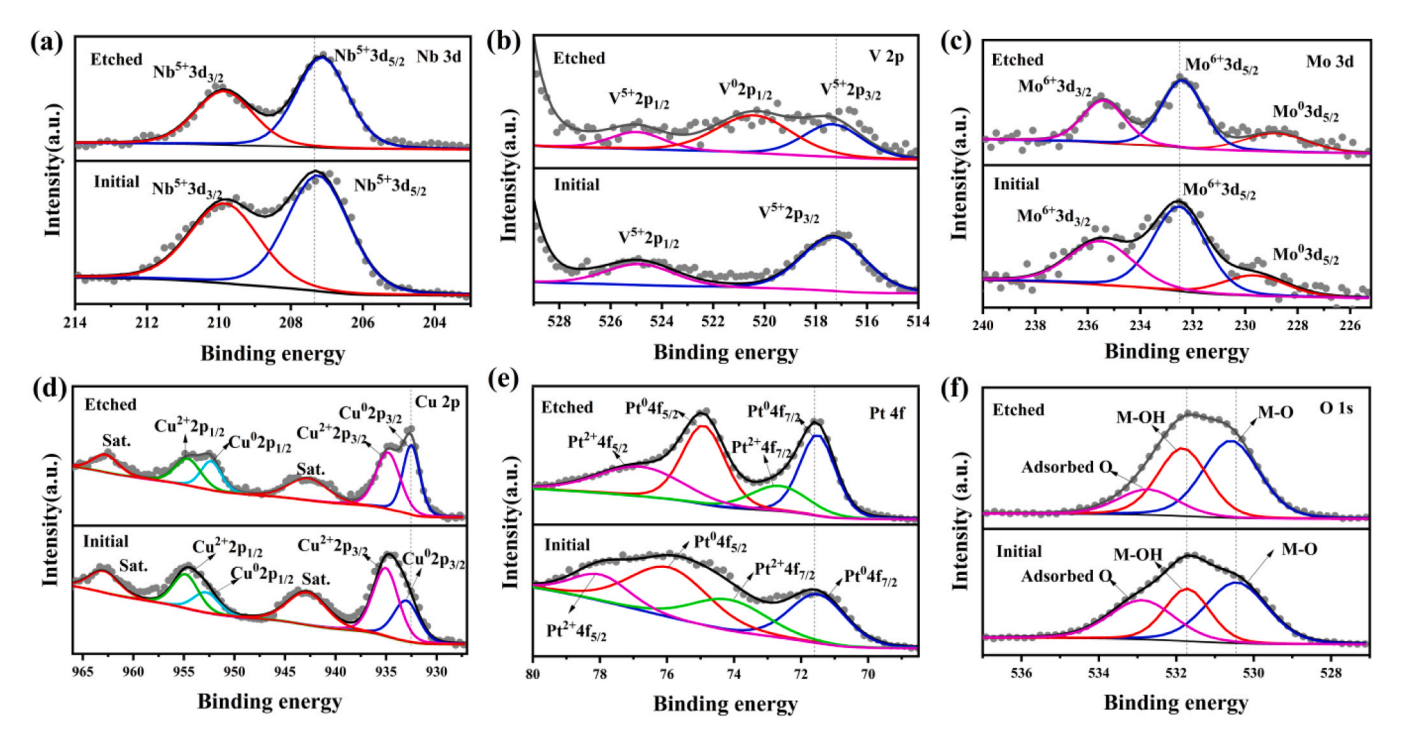


Fig. 3. High resolution XPS patterns of (a) Cu 4 f, (b) Pt 4 f, (c) Mo 3d, (d) Nb 3d, (e) V 2p, and (f) O 1 s spectra for the Nb-V-Mo-Pt-Cu HEA before and after the acid treatment.

Bin Liu et al. Next Materials 8 (2025) 100818

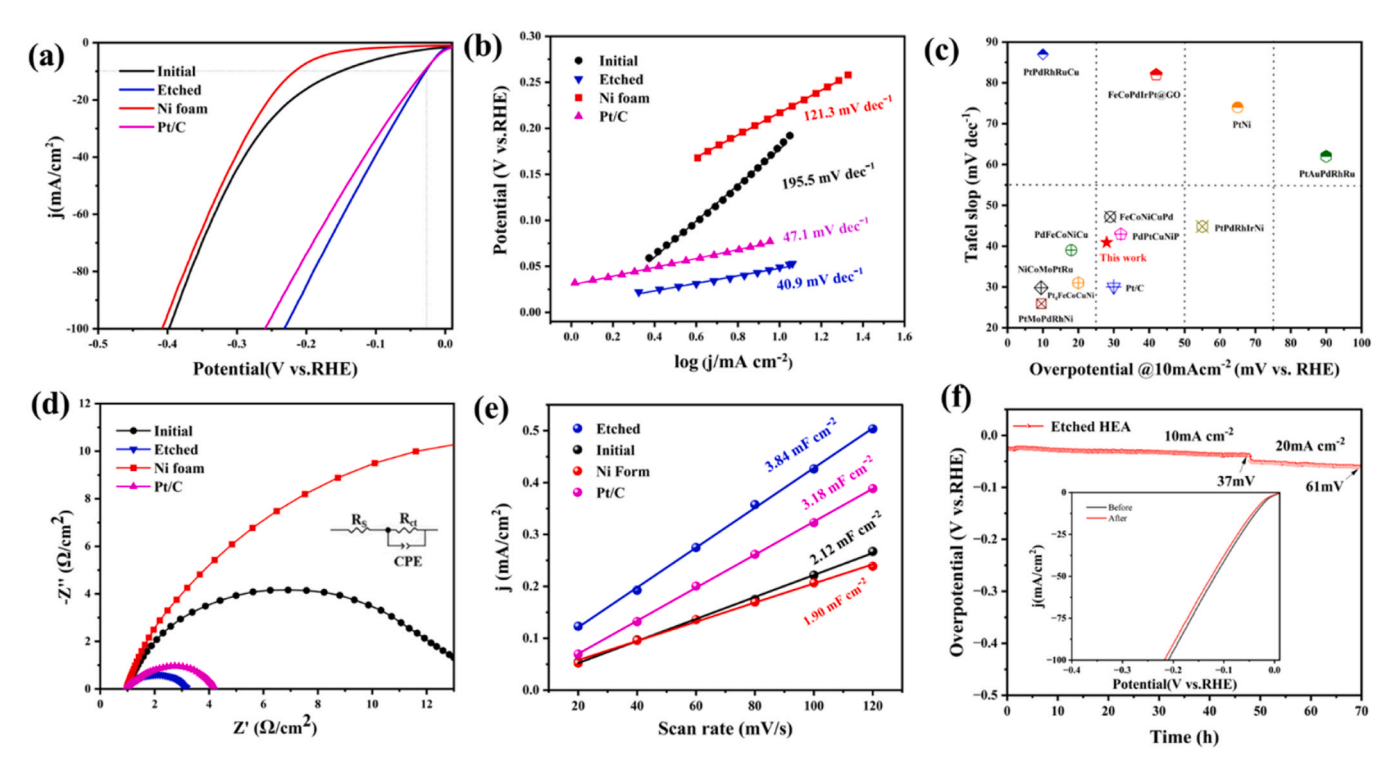


Fig. 4. (a) IR-corrected LSV polarization curves of the initial and acid-etched HEA, Pt/C, and Ni foam in 1.0 M KOH solution. (b) Tafel plots from the polarization curves. (c) Tafel slope and overpotential at 10 mA cm $^{-2}$  of the acid-etched HEA, comparing with the representative HER catalysts. (d) Electrochemical impedance spectroscopy (EIS). (e) The double-layer capacitance ( $C_{dl}$ ). (f) Stability test of the acid-etched HEA at 10 mA cm $^{-2}$  and 20 mA cm $^{-2}$ , the inset is the polarization curves of the HEA before and after stability test.

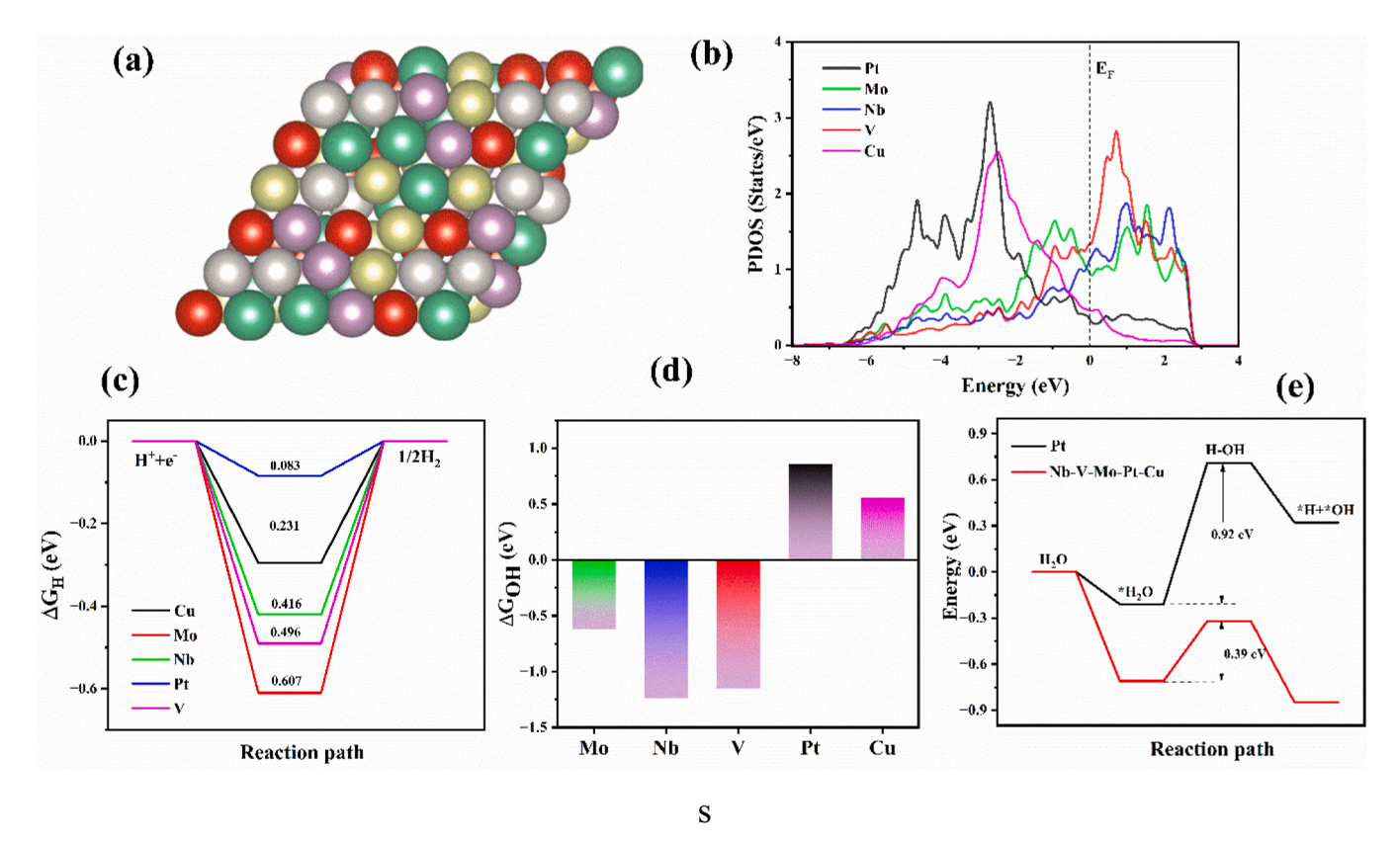


Fig. 5. (a) The atomic configuration of the HEA. (b) The PDOSs of each element on the acid-etched HEA surface. (c) Gibbs free energy profiles of H\* adsorption  $(\Delta G_{H^o})$  on various catalytic sites of the HEA surface. (d) Gibbs free energy profiles of HO\* adsorption  $(\Delta G_{HO^*})$  on various catalytic sites of the HEA surface. (e) Reaction energy for water dissociation on the pure Pt and HEA surfaces.

the initial HEA and compared to the Pt/C catalyst, which demonstrates that the overpotential changes were not related to the geometric surface area. In addition to the catalytic activity , the acid-etched HEA also exhibits high catalytic stability. As depicted in Fig. 4 f, the overpotential remains nearly stable (37 mV) after persistently electrolyzing over 48 h at a current density of 10 mA cm $^{-2}$  in 1.0 M KOH solution, and slowly shifts to 61 mV after further continuous electrolysis for about 24 h at a current density of 20 mA cm $^{-2}$ . Moreover, we examined the structure stability of HEA catalyst after stability test (Figure S7). The surface morphology and crystal structure of this HEA catalyst maintain well, and the atomic percentages are well consistent with that of the catalyst before the stability test (Table S1), indicating good stability of this HEA catalyst for HER in alkaline conditions.

#### 2.4. Density functional theory calculations

Figs. 5a and 5b present the atomic configuration model of the HEA and calculated density of states (PDOSs) projected on each atom, respectively. The Pt 5d and Cu 3d orbitals mainly occupy the bands far below from the Fermi level (E<sub>F</sub>), while the Nb 4d, V 3d and Mo 4d orbitals dominates the bands near the  $E_{\rm F}$ . The former is beneficial for the dehydrogenation processes in alkaline HER [51] and the latter is of great importance to regulate the electron distribution and accelerate electron transfer [52]. The calculated Gibbs free energies of hydrogen adsorption  $(\Delta G_{H^*})$  at the five catalytic sites are displayed in Fig. 5c. One can see that Pt and Cu sites has the most appealing  $\Delta G_{H^*}$ , especially the Pt site realizes a  $\Delta G_{H^*}$  of only -0.083 eV. This is much higher than those of the Nb (-0.416 eV), V (-0.496 eV), and Mo (-0.607 eV) sites, underlying that the Pt site is most suitable for the absorption/desorption of H\* intermediate. Whereas the weak OH\* adsorption (ΔGOH\*) restrict the H2O dissociation on the Pt site, both the Nb and V sites have stronger OH\* adsorption (Fig. 5e). This can change the charge distribution in the H<sub>2</sub>O molecule, thereby activating the H-O bond and accelerating H2O dissociation kinetics, although excessive OH\* adsorption may cause poisoning and blocking of the active sites. Fortunately, the Mo site with a relatively small  $\Delta G_{OH^*}$  of -0.62 eV, in support of the fast OH\* absorption and desorption. Because of this multisite synergy, the energy barrier for breaking the H-OH bond on the HEA surface is as low as 0.39 eV, which is only around one third that on the Pt surface (0.92 eV). This much reduced energy barrier is presumably responsible for the superior alkaline HER performance in the Nb-V-Mo-Cu-Pt HEA.

# 2.5. Discussion

The acid-etched Nb-V-Mo-Cu-Pt HEA as an efficient alkaline HER electrocatalyst have shown some interesting phenomena. In terms of the surface modification, the Nb-V-Mo-Cu-Pt HEA show high intrinsic catalytic activity after the acid etching, it is different from many reported HEA nanocatalysts, in which the nano-size effect makes them have a large specific surface area to maximize the catalytic activity. In contrast, the acid-etched Nb-V-Mo-Cu-Pt is mainly composed of micrometer size particles, and has a small specific surface area. Thus, we speculate that reducing the size of HEA particles will further improve the catalytic performance. In addition, for the catalytic mechanism, the synergistic effect arising from the compositional elements of HEAs is crucial for the optimization of catalytic activity. We found that removing more V/Nb/ Mo elements can increase Pt active sites, but also impair the synergistic effect and result in a reduced catalytic activity. In fact, the V and Nb elements can effectively change the charge distribution of such HEA and optimize the energy barriers of Mo and Pt active sites for stabilizing OH\* and H\* intermediates. In this regard, the electronegativity difference between the compositional elements may be an important factor to be considered in the future exploration of advanced HEA catalysts, which is also an effective strategy to convert inactive to active sites for electrocatalysis [53,54].

#### 3. Conclusions

In summary, we have developed a low-Pt Nb-V-Mo-Pt-Cu HEA catalyst for the efficient alkaline HER by combining arc melting and acid etching. The as-cast HEA adopts a cubic structure, which is maintained after acid etching without phase separation or element aggregation. Electron microscopy and XPS measurements indicate that the acid etching mainly removes the V and Nb elements while leaves more zerovalence Pt and Cu exposed on the surface. The acid-etched HEA exhibits a superior HER catalytic performance with an ultrasmall overpotential of 28 mV@10 mA cm<sup>-2</sup>, a small Tafel slope of 40.8 mV dec<sup>-1</sup>, and good catalytic stability during continuous electrolysis for about 72 h in 1.0 M KOH electrolyte. These properties greatly outweigh the initial HEA and are comparable favorably to the commercial Pt/C and other classical HER catalysts. Through DFT calculations, we show that the enhanced catalytic performance is due to the significant reduction of energy barrier for breaking the H-OH bond resulting from the synergistic effects of multiple active sites (V, Nb, Mo, Pt). Our study offers a viable strategy to develop advanced HEA catalysts for alkaline HER with potential for low cost and large-scale production.

### CRediT authorship contribution statement

Bin Liu: Conceptualization, Data curation, Formal analysis, Funding acquisition, Project administration, Validation, Writing-original draft, Writing-review & editing. Shiping Chen: Data curation, Formal analysis, Investigation, Methodology. Weihao Tan: Data curation, Investigation, Methodology, Validation. Kezhen Zhang: Investigation, Methodology. Xiao Xu: Formal analysis, Investigation. Kun Dong: Methodology, Software. Lan Yu: Resources, Supervision, Writingreview & editing. Kangcheung Chan: Resources, Funding acquisition, Supervision, Visualization. Zhi Ren: Conceptualization, Formal analysis, Visualization, Validation, Writing-review & editing.

## **Declaration of Competing Interest**

The authors declare that they have no known competing financial interests or personal relationships that could have appeared to influence the work reported in this paper.

#### Acknowledgements

This work was supported by the Yunnan Fundamental Research Projects (Grant No. 202401AT070378), the Hong Kong Scholar Program (XJ2023030), and the Analysis and Testing Foundation of Kunming University of Science and Technology.

#### Appendix A. Supporting information

Supplementary data associated with this article can be found in the online version at doi:10.1016/j.nxmate.2025.100818.

#### References

- F. Dawood, M. Anda, G.M. Shafiullah, Hydrogen production for energy: an overview. Int. J. Hydrog. Energy 45 (2020) 3847–3869.
- [2] T. Capurso, M. Stefanizzi, M. Torresi, S.M. Camporeale, Perspective of the role of hydrogen in the 21st century energy transition, Energ. Convers. Manag. 251 (2022) 114898.
- [3] K. Kannaiyan, G.S. Lekshmi, S. Ramakrishna, M. Kang, V. Kumaravel, Perspectives for the Green hydrogen energy-based economy, Energy 284 (2023) 129358.
- [4] B. You, Y. Sun, Innovative strategies for electrocatalytic water splitting, Acc. Chem. Res. 51 (2018) 1571–1580.
- [5] X. Gao, Y. Chen, Y. Wang, L. Zhao, X. Zhao, J. Du, H. Wu, A. Chen, Next-generation Green hydrogen: progress and perspective from electricity, catalyst to electrolyte in electrocatalytic water splitting, NanoMicro Lett. 16 (2024) 237.
- [6] N. Mahmood, Y. Yao, J.W. Zhang, L. Pan, X. Zhang, J.J. Zou, Electrocatalysts for hydrogen evolution in alkaline electrolytes: mechanisms, challenges, and prospective solutions, Adv. Sci. 5 (2018) 1700464.

Bin Liu et al. Next Materials 8 (2025) 100818

- [7] M. Lao, P. Li, Y. Jiang, H. Pan, S.X. Dou, W. Sun, From fundamentals and theories to heterostructured electrocatalyst design: an in-depth understanding of alkaline hydrogen evolution reaction, Nano Energy 98 (2022) 107231.
- [8] A. Eftekhari, Electrocatalysts for hydrogen evolution reaction, Int. J. Hydrog. Energy 42 (2017) 11053–11077.
- [9] J. Zhu, L. Hu, P. Zhao, L.Y.S. Lee, K. Wong, Recent advances in electrocatalytic hydrogen evolution using nanoparticles, Chem. Rev. 120 (2020) 851–918.
- [10] X. Wang, Y. Zheng, W. Sheng, Z.J. Xu, M. Jaroniec, S.Z. Qiao, Strategies for design of electrocatalysts for hydrogen evolution under alkaline conditions, Mater. Today 36 (2020) 125–138.
- [11] Z.C. Yao, T. Tang, Z. Jiang, L. Wang, J.S. Hu, L.J. Wan, Electrocatalytic hydrogen oxidation in alkaline media: from mechanistic insights to catalyst design, ACS nano 16 (2022) 5153–5183.
- [12] C. Lim, A.R. Fairhurst, B.J. Ransom, D. Haering, V.R. Stamenkovic, Role of transition metals in pt alloy catalysts for the oxygen reduction reaction, ACS Catal. 13 (2023) 14874–14893.
- [13] G. Gao, G. Zhu, X. Chen, Z. Sun, A. Cabot, Optimizing Pt-based alloy electrocatalysts for improved hydrogen evolution performance in alkaline electrolytes: a comprehensive review, ACS nano 17 (2023) 20804–20824.
- [14] P. Xie, Y. Yao, Z. Huang, Z. Liu, J. Zhang, T. Li, G. Wang, R. Shahbazian-Yassar, L. Hu, C. Wang, Highly efficient decomposition of ammonia using High-Entropy alloy catalysts, Nat. Commun. 10 (2019) 4011.
- [15] Y. Yao, Z. Liu, P. Xie, Z. Huang, T. Li, D. Morris, Z. Finfrock, J. Zhou, M. Jiao, J. Gao, et al., Computationally aided, entropy-driven synthesis of highly efficient and durable multi-elemental alloy catalysts, Sci. Adv. 6 (2020) eaaz0510.
- [16] E.P. George, D. Raabe, R.O. Ritchie, High-entropy alloys, Nat. Rev. Mater. 4 (2019) 515-534
- [17] D.B. Miracle, O.N. Senkov, A critical review of high entropy alloys and related concepts, Acta Mater. 122 (2017) 448–511.
- [18] J.-T. Ren, L. Chen, H.-Y. Wang, Y. Z.-Y, High-entropy alloys in electrocatalysis: from fundamentals to applications, Chem. Soc. Rev. 52 (2023) 8319–8373.
- [19] F. Lyu, C. Liu, S. Zeng, X. Bu, Y. Chen, Z. Jia, Y. Xie, L. Sun, Z. Mao, J. Shen, G. Li, J. Luan, Y. Yan, L. Yao, L. Li, X. Wang, G. Wu, Y. Li, J. Lu, Boosting hydrogen evolution activity: next-nearest oxygen coordination in dual-phase suprananostructured multiprincipal element alloy catalysts, Energy Environ. Sci. 17 (2024) 7908–7918.
- [20] A. Ahmad, A. Nairan, Z. Feng, R. Zheng, Y. Bai, U. Khan, J. Gao, Unlocking the potential of high entropy alloys in electrochemical water splitting: a review, Small 20 (2024) 2311929.
- [21] G. Zhang, K. Ming, J. Kang, Q. Huang, Z. Zhang, X. Zheng, X. Bi, High entropy alloy as a highly active and stable electrocatalyst for hydrogen evolution reaction, Electrochim. Acta 279 (2018) 19–23.
- [22] Y. Li, Z. Yao, W. Gao, W. Shang, T. Deng, J. Wu, Nanoscale design for high entropy alloy electrocatalysts, Small 20 (2024) 2310006.
- [23] C. Deng, T. Wang, P. Wu, W. Zhu, S. Dai, High entropy materials for catalysis: a critical review of fundamental concepts and applications, Nano Energy 120 (2024) 109153.
- [24] Y. Yao, Z. Huang, P. Xie, S.D. Lacey, R.J. Jacob, H. Xie, F. Chen, A. Nie, T. Pu, M. Rehwoldt, D. Yu, M.R. Zachariah, C. Wang, R. Shahbazian-Yassar, J. Li, L. Hu, Carbothermal shock synthesis of high-entropy-alloy nanoparticles, Science 359 (2018) 1489.
- [25] S. Gao, S. Hao, Z. Huang, Y. Yuan, S. Han, L. Lei, X. Zhang, R.S. Yassar, J. Lu, Synthesis of high-entropy alloy nanoparticles on supports by the fast-moving bed pyrolysis, Nat. Commun. 11 (2020) 2016.
- [26] K. Zeng, J. Zhang, W. Gao, L. Wu, H. Liu, J. Gao, Z. Li, J. Zhou, T. Li, Z. Liang, B. Xu, Y. Yao, Surface-decorated high-entropy alloy catalysts with significantly boosted activity and stability, Adv. Funct. Mater. 32 (2022) 2204643.
- [27] I. McCue, E. Benn, B. Gaskey, J. Erlebacher, Dealloying and dealloyed materials, Annu. Rev. Mater. Res. 46 (2016) 263–286.
- [28] Z. Jin, J. Lv, H. Jia, W. Liu, H. Li, Z. Chen, X. Lin, G. Xie, X. Liu, S. Sun, H.J. Qiu, Nanoporous Al-Ni-Co-Ir-Mo high-entropy alloy for record-high water splitting activity in acidic environments, Small 15 (2019) 1904180.
- [29] A.L. Maulana, P.C. Chen, Z. Shi, Y. Yang, C. Lizandara-Pueyo, F. Seeler, H. D. Abruña, D. Muller, K.S. Arndt, P. Yang, Understanding the structural evolution of IrFeCoNiCu high-entropy alloy nanoparticles under the acidic oxygen evolution reaction, Nano Lett. 23 (2023) 6637–6644.
- [30] D.J.M. King, S.C. Middleburgh, A.G. McGregor, M.B. Cortie, Predicting the formation and stability of single phase high-entropy alloys, Acta Mater. 104 (2016) 172–179.
- [31] X. Xu, W. Yang, H. Song, J. Wang, L. Yu, Z. Ren, B. Liu, Structural sequence and superconductivity in high-entropy Mo-W-Re-Ru-Pd alloys, Scr. Mater. 243 (2024) 115986.

[32] R. Li, X. Liu, W. Liu, Z. Li, K.C. Chan, Z. Lu, Design of hierarchical porosity via manipulating chemical and microstructural complexities in High-Entropy alloys for efficient water electrolysis, Adv. Sci. 9 (2022) 2105808.

- [33] B. Liu, J. Wu, Y. Cui, Q. Zhu, G. Xiao, S. Wu, G. Cao, Z. Ren, Superconductivity in cubic A15-type V-Nb-Mo-Ir-Pt high-entropy alloys, Front. Phys. 9 (2021) 651808.
- [34] H. Liu, H. Qin, J. Kang, L. Ma, G. Chen, Q. Huang, Z. Zhang, E. Liu, H. Lu, J. Li, N. N. Zhao, A freestanding nanoporous NiCoFeMoMn high-entropy alloy as an efficient electrocatalyst for rapid water splitting, Chem. Eng. J. 435 (2022) 134898
- [35] Y. Wang, T. Wang, H. Arandiyan, G. Song, H. Sun, Y. Sabri, C. Zhao, Z. Shao, S. Kawi, Advancing catalysts by stacking fault defects for enhanced hydrogen production: a review, Adv. Mater. 36 (2024) 2313378.
- [36] X. Zhang, Y. Yang, Y. Liu, Z. Jia, Q. Wang, L. Sun, L. Zhang, J. Kruzic, J. Liu, B. Shen, Defect engineering of a High-Entropy metallic glass surface for High-Performance overall water splitting at Ampere-Level current densities, Adv. Mater. 35 (2023) 2303439.
- [37] P. Li, X. Wan, J. Su, W. Liu, Y. Guo, H. Yin, D. Wang, A single-phase FeCoNiMnMo high-entropy alloy oxygen evolution anode working in alkaline solution for over 1000h, ACS Catal. 12 (2022) 11667–11674.
- [38] J.T. Ren, L. Chen, H.Y. Wang, Z.Y. Yuan, Non-precious metal high-entropy alloys with d-d electron interactions for efficient and robust hydrogen oxidation reactions in alkaline media, Inorg. Chem. Front. 11 (2024) 2029–2038.
- [39] X. Han, Q. Chen, Q. Chen, Q. Wu, Z. Xu, T. Zheng, W. Li, D. Cui, Z. Duan, J. Zhang, J. Li, H. Li, Z. Wang, J. Wang, Z. Xia, Eutectic dual-phase microstructure modulated porous high-entropy alloys as high-performance bifunctional electrocatalysts for water splitting, J. Mater. Chem. A 10 (2022) 11110.
- [40] Y. Kang, O. Cretu, J. Kikkawa, K. Kimoto, H. Nara, A.S. Nugraha, H. Kawamoto, M. Eguchi, T. Liao, Z. Sun, T. Asahi, Y. Yamachi, Mesoporous multimetallic nanospheres with exposed highly entropic alloy sites, Nat. Commun. 14 (2023) 4182
- [41] Y. Wang, N. Gong, H. Liu, W. Ma, K. Hippalgaonkar, Z. Liu, Y. Huang, Ordering-Dependent hydrogen evolution and oxygen reduction electrocatalysis of High-Entropy intermetallic Pt<sub>4</sub>FeCoCuNi, Adv. Mater. 35 (2023) 2302067.
- [42] M. Wei, Y. Sun, J. Zhang, F. Ai, S. Xi, J. Wang, High-entropy alloy nanocrystal assembled by nanosheets with d-d electron interaction for hydrogen evolution reaction, Energy Environ. Sci. 16 (2023) 4009.
- [43] G. Feng, Y. Pan, D. Su, D. Xia, Constructing fully-active and ultra-active sites in high-entropy alloy nanoclusters for hydrazine oxidation-assisted electrolytic hydrogen production, Adv. Mater. 36 (2024) 2309715.
- [44] G. Zhao, K. Lu, Y. Li, F. Lu, P. Gao, B. Nan, L. Li, Y. Zhang, P. Xu, X. Liu, L. Chen, An efficient and stable high-entropy alloy electrocatalyst for hydrogen evolution reaction, Chin. J. Catal. 62 (2024) 156–165.
- [45] Y. Wang, B. Yu, M. He, Z. Zhai, K. Yin, F. Kong, Z. Zhang, Eutectic-derived high-entropy nanoporous nanowires for efficient and stable water-to-hydrogen conversion. Nano Res. 5 (2022) 4820–4826.
- [46] Z.J. Zhang, N. Yu, Y.L. Dong, G. Han, H. Hu, Y.M. Chai, B. Dong, High entropy catalysts in electrolytic water splitting: a review from properties to applications, Chem. Eng. J. 498 (2024) 155736.
- [47] M. Li, C. Huang, H. Yang, Y. Wang, X. Song, T. Cheng, J. Jiang, Y. Lu, M. Liu, Q. Yuan, Z. Ye, Z. Hu, H. Huang, Programmable synthesis of high-entropy nanoalloys for efficient ethanol oxidation reaction, ACS nano 17 (2023) 13659–13671.
- [48] X. Yan, Y. Zhou, S. Wang, Nano-High entropy materials in electrocatalysis, Adv. Funct. Mater. 35 (2025) 2413115.
- [49] Y. Jiang, J. Leng, S. Zhang, T. Zhou, M. Liu, S. Liu, Y. Gao, J. Zhao, L. Yang, L. Li, W. Zhao, Modulating water splitting kinetics via charge transfer and interfacial hydrogen spillover effect for robust hydrogen evolution catalysis in alkaline media, Adv. Sci. 10 (2023) 2302358.
- [50] N.K. Shrestha, S.A. Patil, J. Han, S. Cho, A.I. Inamdar, H. Kim, H. Im, Chemical etching induced microporous nickel backbones decorated with metallic fe@ hydroxide nanocatalysts: an efficient and sustainable OER anode toward industrial alkaline water-splitting, J. Mater. Chem. A 10 (2022) 8989–9000.
- [51] H. Li, Y. Han, H. Zhao, W. Qi, D. Zhang, Y. Yu, W. Cai, S. Li, J. Lai, B. Huang, L. Wang, Fast site-to-site electron transfer of high-entropy alloy nanocatalyst driving redox electrocatalysis, Nat. Commun. 11 (2020) 5437.
- [52] C. Zhan, Y. Xu, L. Bu, H. Zhu, Y. Feng, T. Yang, Y. Zhang, Z. Yang, B. Huang, Q. Shao, X. Huang, Subnanometer high-entropy alloy nanowires enable remarkable hydrogen oxidation catalysis, Nat. Commun. 12 (2021) 6261.
- [53] H. Zhu, S. Sun, J. Hao, Z. Zhuang, et al., A high-entropy atomic environment converts inactive to active sites for electrocatalysis, Energy Environ. Sci. 16 (2023) 619–628
- [54] J. Hao, Z. Zhuang, K. Cao, G. Gao, C. Wang, F. Lai, S. Lu, P. Ma, W. Dong, T. Liu, M. Du, H. Zhu, Unraveling the electronegativity-dominated intermediate adsorption on high-entropy alloy electrocatalysts, Nat. Commun. 13 (2022) 2662.